Available online at www.sciencedirect.com

ScienceDirect

materialstoday: PROCEEDINGS

Materials Today: Proceedings 3S (2016) S145 – S152

Proceedings of the International Conference on Diamond and Carbon Materials

Surface Brillouin scattering in ion-implanted chemical vapor deposited diamond.

I. Motochi*, B. A. Mathe, S. R. Naidoo and T. E. Derry

Materials Physics' Research Institute, DST/ NRF Centre of Excellence in Strong Materials and School of Physics, University of the Witwatersrand, Wits 2050, Johannesburg, South Africa.

Abstract

Acoustic waves occurring within an ion-damaged region of CVD diamond were studied using surface Brillouin scattering (SBS). By indirect scattering, the surface acoustic wave (SAW)-like mode of pure diamond, as well as those of carbon ion implanted diamonds to fluences of $1.0x10^{16}$ ions/cm^2 and $1.5x10^{16}$ ions/cm^2 were measured. Pristine diamond had a shear horizontal wave velocity of ≈12500 m/s and the irradiated diamonds showed a shear velocity of ≈12300 m/s. A necessary condition for observing Brillouin spectra via indirect scattering in a transparent medium is shown to be an optically smooth back surface.

Selection and Peer-review under responsibility of the chairs of the International Conference on Diamond and Carbon Materials 2014.

Keywords: Diamond; ion-implantation; surface Brillouin scattering; surface acoustic wave (SAW),

1. Introduction

Brillouin light scattering (BLS) is a well-established technique for determination of the elastic properties of solids, this being achieved by measuring the frequency shifts of the scattered light induced by the velocities of the respective thermally-induced acoustic waves [1]. The technique has the advantage of being non-contact and non-destructive and measurements can also be made as a function of temperature. Early work in the field was largely restricted to the study of bulk acoustic waves in near transparent materials [2,3] In these cases the primary light scattering mechanism was that of elasto-optic effect, in which dynamic fluctuations in the strain field in the bulk of

Selection and Peer-review under responsibility of the chairs of the International Conference on Diamond and Carbon Materials 2014.
doi:10.1016/j.matpr.2016.02.025

the material bring about fluctuations in the dielectric constant, and hence the refractive index. Provided that the samples had a low degree of surface roughness to avoid parasitic scattering, relatively low contrast Fabry-Pérot interferometers were able to detect the scattered light associated with these bulk modes whose frequencies are sufficiently separated from those of the intense elastically scattered light. Under these somewhat restrictive conditions a considerable body of work emerged including studies of crystalline solids, glasses, and polymers [4].

Alternative methods which have proved successful for SBS in transparent materials use scattering geometries with a reflecting substrate as discussed by Jiménez-Riobóo and Belmahi [5], Krüger *et al* [6] and Signoriello *et al* [7]. Guerette and Huang [8] used a Pt plate to provide a reflective surface. The present study sought to determine if as-implanted diamond had different elastic properties to those of pristine specimens using scattering geometry similar to Krüger *et al* [6]. A smooth finish of an Al sample holder provided the reflecting surface. We report on the effects of the back surface morphology and its effects on the spectra observed in pristine and ion-implanted unannealed diamond.

2. Experimental

The samples used were synthetic type IIa single crystal CVD diamonds supplied by Element Six. They had a surface roughness of Ra<30 nm as-supplied and measured 3x3x0.5 mm^3 having a (100) surface in the 3x3 faces. The sample properties are described in table 1.

Table 1: Samples description

Sample	Carbon ion-implant	Polished surfaces	Fluence (ions/cm^2)
1	None	Both	
2	Multiple energy	Both	$1.0x10^{16}$
3	Single energy implanted (150 keV)	Both	$1.5x10^{16}$
4	None	One	
5	Single energy implanted (150 keV)	One	$1.5x10^{16}$

Ion implantation was performed with a Varian 200-20A2F ion implanter located at iThemba LABs (Gauteng), South Africa. All implantations were performed at room temperature with the ion beam uniformly scanned over the sample surface with a beam current of ≈1.0 μA/cm^2. The samples were ion implanted with ^{12}C ions. A damaged layer of thickness ≈ 230 nm was predicted by TRIM 2008 [9] simulation using a displacement energy of 45 eV.

SBS measurement was performed at room temperature. An Ar^+ laser fitted with an intra-cavity etalon provided the p-polarized excitation beam of wavelength 514.5 nm and power of about 400 mW. The beam intensity was reduced to <60 mW at the sample, considered sufficiently low not to cause any significant heating. The inelastically scattered light was analysed by a 3+3 pass Sandercock-type tandem Fabry Pérot interferometer characterized by a finesse of about 100 and a contrast ratio higher than 10^{10} [10]. Incident light impinged on the un-implanted side as shown in the schematic setup in figure 1(i). The backscattering geometry that is suitable for transparent materials shown in Figure 1(ii) was used in the analysis of observed modes [7]. When an incident optical beam of angular

frequency Ω_i, wavelength λ_i and wavevector $\boldsymbol{q}_i$ ($|\boldsymbol{q}_i|=2\pi/\lambda_i$) impinges on the surface of a sample at incidence angle θ, it is refracted with wavevector $\boldsymbol{q}'_i$ at angle θ′, to the normal, with $\boldsymbol{q}'_i = n|\boldsymbol{q}_i|$, n being the refractive index. Upon interaction with a bulk acoustic wave (BAW) of wavevector $\boldsymbol{k}_b$ and angular frequency ω($|\boldsymbol{k}_b|$), where $\omega= \omega_l=v_l|\boldsymbol{k}_b|$ or $\omega= \omega_t=v_t|\boldsymbol{k}_b|$ it is scattered into an optical wave of angular frequency Ω_s, and wavevector $\boldsymbol{q}'_s$, which then emerges with wavevector $\boldsymbol{q}_s$. Conservation of momentum and energy coupled with the wide difference between the velocities of sound and light, imply that $|\boldsymbol{q}'_i|=|\boldsymbol{q}'_s|$. The scattering geometry determines the directions of $\boldsymbol{q}_i$ and $\boldsymbol{q}_s$ and thus the selects the acoustic wavevector $\boldsymbol{k}_b$ being probed. In backscattering geometry like one used in this study $\boldsymbol{q}_s = -\boldsymbol{q}_i$. Three different probable scattering scenarios, explained from figure 1(ii) are summarized from Beghi *et al* [11] and Signoriello *et al* [7]. In the first case, incident light of angular frequency Ω_i is scattered by a surface wave of wavevector $\boldsymbol{k}_s$ (phonons at zone A (back) and S (front) in figure 1(i)) that is parallel to the surface. There is lack of translational invariance in the direction normal to the surface (thus $(\boldsymbol{q}_s)_{\|} = (\boldsymbol{q}_i)_{\|} \pm \boldsymbol{k}_s$) hence upon refraction $|\boldsymbol{q}'_{\|} = \boldsymbol{q}_{\|}$, Snell's law breaks down, there is no distinction between $\boldsymbol{q}'$ and $\boldsymbol{q}$, and the value of the refractive index is irrelevant in the calculation of the surface acoustic wave (SAW) velocity of the material. A consideration of momentum and energy conservation of the phonon wave vectors, results in the scattered radiation that contains a dispersive doublet occurring at frequency shifts given by,

$$\Omega_s - \Omega_i = \pm\omega(|\boldsymbol{k}_s|) = \pm 2|\boldsymbol{q}_i|_{\|} v_R = \pm 2\pi(2v_R \sin\theta/\lambda_i) \quad (1)$$

where v_R is the velocity of a SAW, λ_i the wavelength of the incident photon, and ω the acoustical angular frequency.

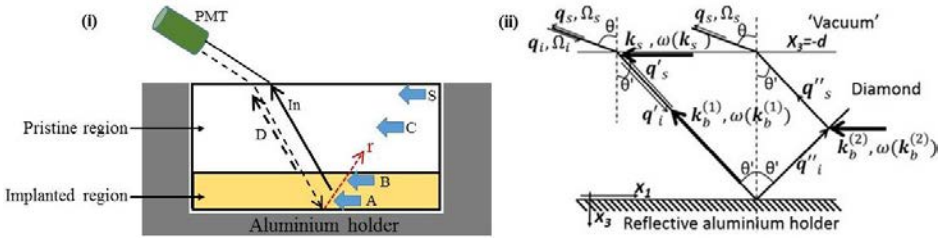

Figure 1: (i) Al holder able to freely hold the diamond samples and to provide a reflecting surface. A and S are opposite faces of the surface/ near surface zones of the sample, the reflected photon 'r' is scattered by phonons indirectly along zones B and C while along D the photons are scattered directly. (ii) Back scattering geometry which represents a transparent sample held on a reflective holder and closely follows that presented in ref. [7]. Thin arrows represent optical wave vectors while thick arrows show acoustic wave vectors of bulk ($\boldsymbol{k}_b$) and surface ($\boldsymbol{k}_s$) acoustic waves. Ω_i, Ω_s are the incident and scattered optical angular frequencies; ω is the acoustical angular frequency; $\boldsymbol{q}_i$, $\boldsymbol{q}_s$ are the incident and scattered optical wave vectors in "vacuum"; $\boldsymbol{q}'_i$, $\boldsymbol{q}'_s$, $\boldsymbol{q}''_i$, $\boldsymbol{q}''_s$ are the incident and reflected optical wave vectors inside the medium before and after reflection, respectively; θ is the incident and scattering angles of the optical wave vector in "vacuum" while θ′ is the refracted and reflected angles of the acoustical wave vector at the sample holder [10].

The second case, scattering directly by a bulk wave of wavevector $\boldsymbol{k}_b^{(1)}$ (along D) in which case $\boldsymbol{q}'_s = -\boldsymbol{q}'_i$, hence $|\boldsymbol{k}_b^{(1)}|=2|\boldsymbol{q}'_i|$ and the spectrum of the scattered radiation contains a doublet at angular frequency shifts;

$$\Omega_s - \Omega_i = \pm\omega(|\boldsymbol{k}_b^{(1)}|) = \pm 2|\boldsymbol{q}_i|_{\|} v = \pm 2\pi(2nv/\lambda_i) \quad (2)$$

Where $v = v_l$ or $v = v_t$, the doublet are non-dispersive and depend on the refractive index of the medium. The third scenario is scattering indirectly by a bulk wave $\boldsymbol{k}_b^{(2)}$, (along zones B to C in figure 1(i)). Scattering necessarily occurs after reflection at the back surface of the transparent sample at zone A. Again, there is invariance of the

parallel component of the wavevector upon refraction, this implies that $\boldsymbol{k}_b^{(2)} = \boldsymbol{k}_s$, the scattered radiation occurs at frequency shifts given by equation (3), yielding dispersive modes:

$$\Omega_s - \Omega_i = \pm\omega(|\boldsymbol{k}_b^{(2)}|) = \pm 2|\boldsymbol{q}_i|_{\|} v = \pm 2\pi(2nv \sin\theta/\lambda_i) \quad (3)$$

where v is the modes' phase velocity consisting of $v = v_l$ (longitudinal modes) and $v = v_t$ (two transverse modes, fast and slow transverse), that does not depend on the refractive index of the sample. In this investigation, the region of interest was the ion damaged region ($\approx$230 nm) of diamond shown in brownish yellow colour in figure 1(i). Thus, emphasis is laid on the phonons characterized by wave vector $\boldsymbol{k}_s$ and $\boldsymbol{k}_b^{(2)}$.

3. Results and discussion

Raman spectroscopy measurements using laser excitation of wavelength 514.5 nm on un-implanted diamond gave the usual narrow first order diamond peak at 1332 cm^{-1} with a FWHM of 1.93 wavenumbers. Measurements after implantation at randomly selected regions show that the samples were uniformly damaged as indicated by a broad peak centred about $\approx$1550 cm^{-1}.

SBS measurements at different angles of incidence were performed and representative spectra from the multiple-energy implant, sample 2 (polished on both surfaces) are shown in figure 2. Samples 1 and 3 bore similar spectra (not shown). The single peak (frequency shift) observed scales with the angle of incidence, showing a SAW-like characteristic. However, featureless spectra were obtained for samples 4 and 5 within the same spectral range (<±55 GHz). Lack of detectable modes was attributed to poor reflectivity at the back unpolished surfaces for these samples, hence no indirect scattering by $\boldsymbol{k}_b^{(2)}$ modes was observed. It was therefore concluded that the observed peaks for samples 1, 2 and 3 originate from scattering by $\boldsymbol{k}_b^{(2)}$ modes after reflection of light at the back surface of the sample and not from a surface ripple mechanism.

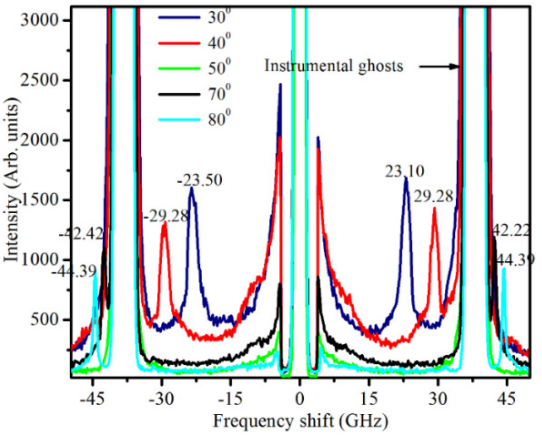

Figure 2: Brillouin spectra for the SAW-like peak for different angles of incidence for sample 2 (colour online).

A plot of frequency shift with incidence angle (for samples 1, 2 and 3) is shown in figure 3 and satisfies the relation $v_{SAW} = \upsilon\lambda_i/(2 \sin\theta_i)$, where v_{SAW} is the phase velocity of SAW-like mode, υ is the frequency shift, λ_i is the incident laser wavelength and θ_i is the incident angle. The gradient of the plot of figure 3 gives the sound velocity of

this mode. A cursory examination of the gradient calculated by this plot may suggest that the single implanted diamond had a higher sound velocity (12700±70 m/s) than that of the pristine (11900±60 m/s) and that of the multiple energy implanted (12000±120 m/s) diamonds. However, one needs to account for the azimuthal dependency first before

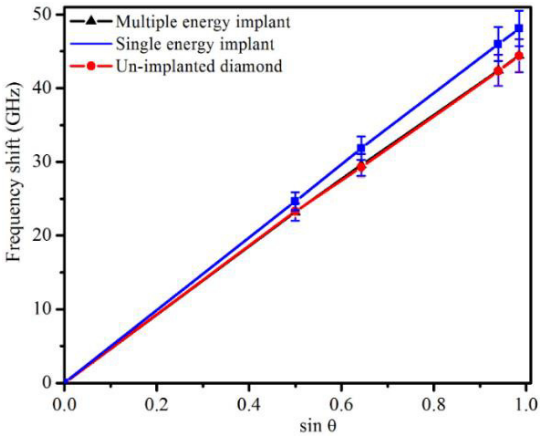

Figure 3: Frequency shifts scaling with the sine of the angle of incidence for samples 1, 2 and 3 (colour online).

making on the values obtained from the gradient. In anisotropic media like diamond, the sound velocity is direction dependent. In table 2, the average sound velocities were obtained from measurements taken at a constant incidence angle of 70^o and plotted in figure 4, taking into account the azimuth orientation of the samples. It can be observed that though the irradiated diamond had sufficient radiation damage, it still retained a strong degree of anisotropy, showing a fourfold symmetry for the (100) surface as described by Flannery *et al* [12] (see figure 4). The experimental values were fitted with a sine function of the form $A=v_o \sin \theta_A$; where A is the variation of the sound velocity as the azimuth angle varies, v_o is the average sound velocity in the medium and θ_A is the azimuth angle.

The average sound velocities from Table 2 show that the pristine diamond has the highest velocity while the heavily implanted (single-energy implant) diamond has the lowest. From the setup and geometry shown in figure 1, that governed photon-phonon interaction in this study, the scattered photons due to $\boldsymbol{k}_b^{(2)}$ transited through the damaged layer in samples 2 and 3. This argument is supported by transmission measurements which showed a considerable decrease in transmission of the 514.5 nm light from 69.3% in pristine diamond to 15% in the as-implanted diamonds. Ion implantation for the fluences used in this study causes radiation damage which results in a decrease in density due to lattice expansion [13]. Associated with this extensive damage is a fair amount of stress and strain near the implanted region [14], which makes BLS a suitable technique for the study of changes in elasticity in the material.

Table 2: Rayleigh-like velocities in pristine and near surface damaged diamond

	Un-implanted (Sample 1)	Multiple energy implant (Sample 2)	Single energy implant (Sample 3)
Sound velocity v_o (m/s)	12500 ± 40	12400 ± 30	12300 ± 30
A (m/s)	670 ± 50	620 ± 40	610± 20

The range of sound velocities obtained show that the probed mode is a bulk transverse (shear) wave of diamond mediated by the softer damaged layer hence the slightly lower velocities that was consistent with the level of damage of the sample. There appears to be no soft modes exclusively originating from the as-implanted radiation damaged region owing to lack of distinct interface between the pristine diamond and the radiation damaged region.

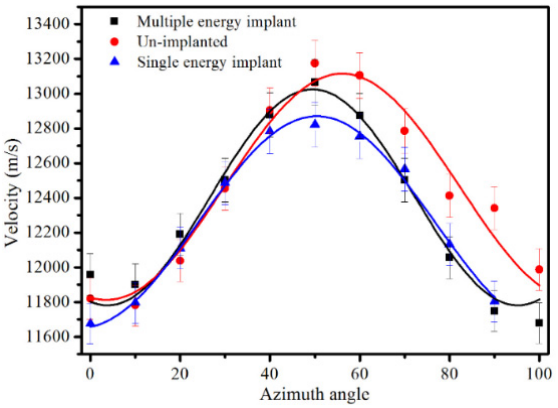

Figure 4: Experimental values of direction dependent SAW-like velocity fitted with a sine function to show preservation of the four-fold symmetry in as-implanted diamond samples 2 and 3 compared to pristine diamond (sample 1) (colour online).

Comparative studies elucidate the fact that the observed peak was likely a transverse mode with a SAW-like characteristic. Jiang *et al* [15] calculated a Rayleigh velocity of 10753 m/s on polycrystalline CVD and in the same report, they measured an experimental value of 10326±470 m/s using SBS. Apart from the Rayleigh mode they were also able to measure the velocities of slow and fast transverse modes on the (110) surface but only one transverse mode on the (100) surface. They reported the slow and fast transverse velocities to be at 11582±380 and 12437±250 m/s, respectively. Philip *et al* [16] reported a Rayleigh velocity of 10750±80 m/s for nanocrystalline diamond of thickness 3.61 μm measured using broadband surface acoustic wave pulses. Djemia *et al* [17] obtained a Rayleigh velocity of 10800±300 m/s on polycrystalline diamond using SBS. Whitefield *et al* [18] asserted that the Rayleigh mode of diamond lies in the range 11000-12000 m/s while other researchers like Flannery *et al* [12] have given the transverse velocity of diamond as ≈13000 m/s. The present experimental results are strongly indicative of the dispersive mode of CVD, despite the scattering effect and reflection occurring in the near-surface of the radiation damaged region. Yet, it is worth noting that the scattering geometry that governs the wavevector $\boldsymbol{k}_s$, applies to modes travelling parallel to the surface, for scattering events occurring within the solid angle of the detector optics, partly determined by the width of zones A and B.

Studies were also done using an extended spectral range that enabled observation of bulk modes induced by direct scattering. Non-dispersive longitudinal and transverse peaks were observed in samples 1, 2 and 3. A similar longitudinal peak due to direct scattering was observed in samples 4 and 5 only when light impinged the polished side, spectra from these measurements is shown in figure 5. The mode due to scattering indirectly by a bulk wave $\boldsymbol{k}_b^{(2)}$ was not observed when light impinged on the polished side of samples 4 and 5. This is attributed to the fact

that the Krüger backscattering geometry relies on surface reflectivity of the back surface which was a contrary case in samples 4 and 5, both which were one-surface polished. A rough surface leads to diffuse or no reflection of light, causing phonon wave vector and momentum conservation to break down, thus without any coherent scattering at an interface, no BLS modes are observed.

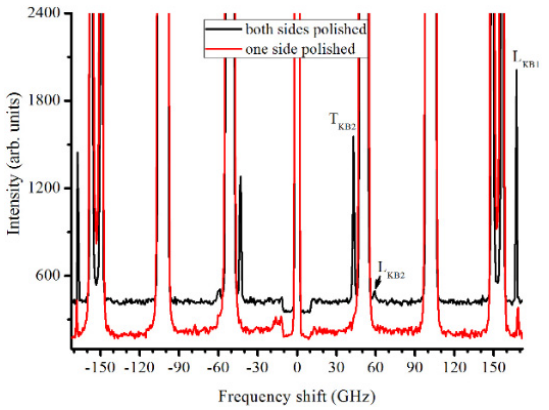

Figure 5: Bulk modes due to direct and indirect scattering for light incident at 60° on samples 1 (black line). Only peaks due to direct scattering were observed in sample 4, light incidence at angle of 70° (red line). T_{KB2} and L_{KB2} are peaks due to indirect scattering from phonon wavevector $\boldsymbol{k}_b^{(2)}$ while L_{KB1} peak is from direct phonon wavevector $\boldsymbol{k}_b^{(1)}$. Spectrum displaced for clarity (colour online).

Peak L_{KB2} was identified as a longitudinal mode with SAW-like characteristics, and its velocity was calculated to be 17615 m/s using the equation $v_{surf} = \upsilon_2\lambda_i/(2 \sin \theta_i)$, where λ=514.5 and θ_i=60°, whilst the mode L_{KB1} was identified as a normal bulk longitudinal mode, its velocity is calculated using $V_{bulk} = \upsilon_1\lambda_i/2n$, where n is the refractive index. The two peaks should have the same velocity since they are the same modes in the same crystal direction. The refractive index $n = (\upsilon_1/\upsilon_2)\sin \theta_i$, when υ_1=167.0 GHz, υ_2=59.8 GHz and θ_i=60° was then determined as 2.418 which is in agreement with the refractive index of CVD diamond, 2.417. Thus, the result confirms the correct assignment of the related modes in the scattering geometry employed in this work, the indirectly scattered $\boldsymbol{k}_b^{(2)}$ and the directly scattered $\boldsymbol{k}_b^{(1)}$ longitudinal modes.

4. Conclusions

This study has demonstrated that in order to measure phonons modes by indirectly scattered light for single crystal diamond using the Krüger backscattering geometry, a polished back surface of the CVD and smooth, reflective metallic support base are necessary conditions. In implanted samples, the sample was positioned such that scattering events occurring in the ion- implanted region could be observed, so that the elasticity information could be gleaned about the radiation damaged region. The lack of a distinct boundary between the radiation damaged region and the pristine diamond presented challenges in obtaining modes exclusive to this region of interest. However, the averaged effect still showed the slight weakening/ softening of the radiation damaged region compared to the pristine diamond. The difference in sound velocities of the SAW-like modes was attributed to

change in lattice structure of the surface region due to radiation damage in the implanted layer and the resulting strain. Additionally, by correlating the respective acoustic modes mediated by direct and indirect scattering geometries, the accurate determination of the refractive index provided validation of the mode assignments made in this study.

The financial support of the African Laser Centre and the DST-NRF Centre of Excellence in Strong Materials (CoE-SM) for the first author towards this research is hereby acknowledged.

References

[1] W. Hayes and R. Loudon, Scattering of Light by Crystals, (Wiley, New York) 1978.

[2] H. Z. Cummins and P.E. Schoen, *Laser Handbook* ed. F.T. Arecchi and E.O. Schulz-Dubois, (North Holland, Amsterdam)1972, pp1029.

[3] R.Vacher and L. Boyer, *Phys. Rev*. B **6** (1982) 639-673.

[4] J.G. Dill, *Rep. Prog. Phys.*, **42 (**1982) 285-334.

[5] R.Jiménez-Riobóo and M. Belmahi, *J. Appl. Phys.* **97**, (2005) 073509.

[6] J.K. Krüger, J. Embs, J. Brierley and R. Jimenez-Riobóo, *J. Phys. D: Appl. Phys.* **31**, (1998) 1913 1917.

[7] G. Signoriello, M. G. Beghi, A. R. Clerici and G. Spinola, *7th Int. Conf. on mechanical and multiphysics simulation and experiments in micro-electronics and micro-systems* EuroSimE, 2003.

[8] M. Guerette and L. Huang, *J. Phys. D: Appl. Phys.* **45**, (2012), 275302.

[9] J. F. Ziegler, J. P. Biersack and M. D. Ziegler, *Q. The Stopping and Range of Ions in Matter.* Chester, Maryland, 21619, USA, 2008, pg 11-7.

[10] P. Djemia, C. Dugautier, T. Chauveau, E. Dogheche, M. I. De Barros and L. Vandenbulcke, *J. Appl. Phys.* **90**, No 8, (2001), 3771-3779.

[11] M.G. Beghi, A.G. Every and P. V. Zinin, in Ultrasonic non-destructive evaluation, Ed. T. Kundu (CRC Boca Raton Fl, 2004, pp.581-651.

[12] C. M. Flannery, M. D. Whitfield and R. B. Jackman, *Semicond. Sci. Technol.* **58**, (2003), S86-S95.

[13] J. F. Prins and T. E. Derry, *Nucl. Instr. And Meth. In Phys. Res. B*. **166-167**, (2000), 364-373.

[14] B. A. Fairchild, S. Rubanov, D. W. M. Lau, M. Robinson, I Suarez-Martinez, N. Marks, A. D. Greentree, D. McCulloth and S. Prawer, *Adv. Mater.* **24**, (2012) 2024-2029

[15] X. Jiang, J. V. Harzer, B. Hillebrands, Ch. Wild, and P. Koidle, *Appl. Phys. Lett.* **59** pp. (1991) 1055–1057.

[16] J. Philip, P. Hess, T. Feygelson, J. E. Butler, S. Chattopadhyay, K. H. Chen, and L. C. Chen, *J. Appl. Phys.* **93** (2003) 2164–2171.

[17] P. Djemia, C. Dugautier, T. Chauveau, E. Dogheche, M. I. Barros, and L. Vandenbulcke, *J. Appl. Phys*. **90(8),** (2001) 3771–3779.

[18] M. D. Whitfield, B. Audic, C. M. Flannery, L. P. Kehoe, C. Johnston, P. R. Chalker and R. B. Jackman, *Diam. Rel. Mater.* **7**, (1998) 533.